

Research on Inter-turn Short-circuit Fault Diagnosis Method Based on High Frequency Voltage Residual for PMSM

Xiaobao Feng, Bo Wang, *IEEE Senior Member*, Chaohui Liu, *IEEE Member*, Jiayun Zeng, and Zheng Wang, *IEEE Senior Member*

Abstract—Inter-turn fault is a serious stator winding short-circuit fault of permanent magnet synchronous machine (PMSM). Once it occurs, it produces a huge short-circuit current that poses a great risk to the safe operation of PMSM. Thus, an inter-turn short-circuit fault (ITSCF) diagnosis method based on high frequency (HF) voltage residual is proposed in this paper with proper HF signal injection. First, the analytical models of PMSM after the ITSCF are deduced. Based on the model, the voltage residual at low frequency (LF) and HF can be obtained. It is revealed that the HF voltage residual has a stronger ITSCF detection capability compared to the LF voltage residual. To obtain optimal fault signature, a 3-phase symmetrical HF voltage is injected into the machine drive system, and the HF voltage residuals are extracted. The fault indicator is defined as the standard deviation of the 3-phase HF voltage residuals. The effectiveness of the proposed ITSCF diagnosis method is verified by experiments on a triple 3-phase PMSM. It is worth noting that no extra hardware equipment is required to implement the proposed method.

Index Terms—Inter-turn short-circuit fault (ITSCF), Permanent magnet synchronous machine (PMSM), High frequency (HF) injection, Voltage residual, Fault diagnosis.

I. INTRODUCTION

PMSM are widely used in military fields, transportation electrification and industrial equipment, which require a high level of reliability for the machine drive system [1]-[3]. The common faults of PMSM can be divided into mechanical

faults and electrical faults, among which stator-related faults account for about 21% of total failures [4]. The insulation of the stator winding is prone to degradation due to excessive heat, vibration and chemical corrosion [5]. Once the insulation is damaged, it may develop into inter-turn fault, phase-to-phase fault and phase-to-ground fault [6], and inter-turn fault is the worst fault which attracts widespread concern. ITSCF usually occurs between several turns of the phase winding, resulting in low impedance of the fault turns. Therefore, a fantastic short-circuit current will be caused by inter-turn fault, which usually reaches ten times of the rated value [7]. The short-circuit current will generate a considerable amount of heat to further damage the winding insulation, causing a vicious cycle until completely breakdown. To solve the problem, prominently efforts have been invested in fault-tolerant machine design [8]-[10], fault-tolerant strategies [11], [12] and fault detection methods [13]-[18]. At present, it is still an irreplaceable protective measure to adopt an appropriate fault diagnosis method to alarm faults and take mitigation measures.

The insulation monitoring and fault diagnosis of stator winding have been widely studied by researchers. As a non-invasive fault detection method, machine current signal analysis (MCSA) [13], [14] achieves ITSCF detection by analyzing the spectrum of machine current and identifying the spectrum signal related to the fault. However, the measured signal is easily influenced by the transient process of the machine, and it is difficult to achieve reliable detection in the actual system. In [15]-[17], the zero-sequence voltage and negative sequence voltage were studied to obtain the fault signature. While these methods can achieve good detection, the measurement of voltage signal requires adding voltage sensors. Besides analyzing the signal directly, the model-based diagnosis method is also employed. In [18], [19], the second harmonic of current residual and voltage residual is used to detect ITSCF. Unlike directly measuring the signal, the model-based method uses the difference between the reference signal and the estimated signal to obtain the residual caused by the fault. Since both the reference signal and the estimated signal are both affected by the ITSCF, the fault signatures of the model-based method are enhanced.

Due to the inter-turn short-circuit that occurs inside the phase winding, a weak fault signal will be generated, especially when only one single-turn short-circuit. It is revealed in [20] that single-turn fault generate the largest fault current with weakest

Manuscript received April 28, 2023; revised June 06 and July 16, 2023; accepted August 29, 2023. Date of publication September 25, 2023; Date of current version September 18, 2023.

This work was supported in part by the Jiangsu Carbon Peak Carbon Neutralization Science and Technology Innovation Special Fund under Grant BE2022032-1; in part by National Natural Science Foundation of China under Grant 52277035, Grant 51937006 and Grant 51907028; in part by the “SEU Zhishan Young Scholars” Program of Southeast University. (*Corresponding author: Bo Wang*)

Xiaobao Feng, Bo Wang and Zheng Wang are with the School of Electrical Engineering, Southeast University, Nanjing 210096, China (e-mail: fengxb_ee@163.com, b.wang@seu.edu.cn, zwang@seu.edu.cn).

Chaohui Liu is with National New Energy Vehicle Technology Innovation Center (NEVC), Beijing 100176, China (e-mail: liuchaohui@nevc.com.cn).

Jiayun Zeng is with Nanjing Engineering Institute of Aircraft System, Aviation Industry Corporation of China, Nanjing 211106, China (e-mail: GraceZavic@163.com).

Digital Object Identifier 10.30941/CESTEMS.2023.00050

featured harmonics. The above-mentioned LF signal-based methods are difficult to detect minor ITSCF. Inspired by rotor position sensorless technology, HF injection strategy has been employed for fault detection. Currently, HF injection methods can be divided into HF voltage injection and HF current injection. In [21], [22], the variations of zero-sequence voltage and phase voltage after HF current injection are used as fault characteristics to detect ITSCF. Nevertheless, the measurement of voltage signals typically requires voltage sensors. For HF voltage injection, it can be divided into two main types. One is to use the sideband harmonics of PWM as the natural HF voltage source and realize ITSCF diagnosis through the change of 3-phase HF ripple currents before and after the fault [23], [24]. Generally, the sideband harmonics at twice the PWM switching frequency are used, which exceeds the sampling frequency of common machine drive system and additional hardware circuits are still needed to process the HF current signals. The other approach is to inject a specially defined HF voltage signal, and 3-phase HF current is then utilized as the fault inductor [25], [26]. However, HF current is not a reliable fault indicator, particularly when the magnitude of the injected signal is not high enough.

By combining the advantages of model-based method and HF injection method, this paper proposes an ITSCF detection method based on HF voltage residual without the addition of hardware equipment. The machine drive system is injected with 3-phase symmetrical HF voltage, which causes HF signals to appear in the reference voltage and estimated voltage. Under normal operating conditions, the HF reference voltage is similar to the HF estimated voltage. However, in the event of ITSCF, there is a significant deviation. The standard deviation of the 3-phase HF voltage residuals is used as the fault indicator to reflect the degree of dispersion. The effectiveness and robustness of the proposed method are demonstrated through extensive experimental tests on a triple 3-phase PMSM. The main contributions are listed as follows:

- 1) It is revealed that the fault diagnosis methods based on voltage residuals can be enhanced under HF.
- 2) The detection of ITSCF is achieved by using HF voltage signal without adding voltage sensor and hardware circuit.
- 3) The diagnosis method has strong robustness, which is not affected by load and parameter changes.

II. FAULT MODEL

ITSCF altered the structure of the stator winding, making the original analytical model unavailable. In order to extract fault symptoms, the governing equations of PMSM models under inter-turn fault conditions are analyzed. Due to the enhancement of fault signatures under HF, the fault model under HF has also been derived.

When inter-turn fault occurs, the winding can be divided into healthy turns and fault turns as shown in Fig. 1. The contact resistance of the fault turn is denoted as R_f . The definitions of resistance, inductance and back electromotive force (EMF) for healthy and faulty turns have also been indicated. Based on the stator winding after ITSCF, the model can be expressed as (1),

where u_{ah} and u_{af} denote the voltages of healthy and faulty turns of phase A, u_{bn} and u_{cn} denote the voltages of phase B and phase C, i_f denotes the fault current, and i_a , i_b and i_c denote the phase current.

$$\mathbf{U}_{yf} = \mathbf{R}_{yf} \mathbf{I}_{yf} + \frac{d(\mathbf{L}_{yf} \mathbf{I}_{yf})}{dt} + \mathbf{e}_{yf} \quad (1)$$

$$\text{where } \mathbf{U}_{yf} = \begin{bmatrix} u_{ah} \\ u_{af} \\ u_{bn} \\ u_{cn} \end{bmatrix}, \mathbf{R}_{yf} = \begin{bmatrix} R_{ah} \\ R_{af} \\ R_s \\ R_s \end{bmatrix}, \mathbf{I}_{yf} = \begin{bmatrix} i_a - i_f \\ i_a \\ i_b \\ i_c \end{bmatrix}, \mathbf{e}_{yf} = \begin{bmatrix} e_{ah} \\ e_{af} \\ e_b \\ e_c \end{bmatrix},$$

$$\mathbf{L}_{yf} = \begin{bmatrix} L_{ah} & M_{hf} & L_{ahb} & L_{ahc} \\ M_{hf} & L_{af} & M_{afb} & M_{afc} \\ M_{ahb} & M_{afb} & L_b & M_{bc} \\ M_{ahc} & M_{afc} & M_{bc} & L_c \end{bmatrix}.$$

The percentage of the number of short-circuit turns to total turns of one phase is typically defined as μ . According to [27], [28], the following relationship between machine parameters and fault turns can be obtained.

$$\begin{cases} R_{ah} = (1-\mu)R_s, R_{af} = \mu R_s \\ L_{ah} = (1-\mu)^2 L_a, L_{af} = \mu^2 L_a, M_{hf} = \mu^2 L_a \\ M_{ahb} = (1-\mu)M_{ab}, M_{afb} = \mu M_{ab} \\ M_{ahc} = (1-\mu)M_{ac}, M_{afc} = \mu M_{ac} \\ e_{ah} = (1-\mu)e_a, e_{af} = \mu e_a \end{cases} \quad (2)$$

Combing (1), (2) and $u_{an} = u_{ah} + u_{af}$, the 3-phase voltage equation after the ITSCF can be derived as:

$$\mathbf{U}_s = \mathbf{R}_s \mathbf{I}_s + \frac{d(\mathbf{L}_s \mathbf{I}_s)}{dt} + \mathbf{e}_s \quad (3)$$

$$\text{where } \mathbf{U}_s = \begin{bmatrix} u_{an} \\ u_{bn} \\ u_{cn} \\ 0 \end{bmatrix}, \mathbf{R}_s = \begin{bmatrix} R_s & 0 & 0 & -\mu R_s \\ 0 & R_s & 0 & 0 \\ 0 & 0 & R_s & 0 \\ \mu R_s & 0 & 0 & -\mu R_s - R_f \end{bmatrix},$$

$$\mathbf{I}_s = \begin{bmatrix} i_a \\ i_b \\ i_c \\ i_f \end{bmatrix}, \mathbf{e}_s = \begin{bmatrix} e_{ah} \\ e_{af} \\ e_b \\ e_c \end{bmatrix}, \mathbf{L}_s = \begin{bmatrix} L_a & M_{ab} & M_{ac} & -\mu L_a \\ M_{ab} & L_b & M_{bc} & -\mu M_{ab} \\ M_{ac} & M_{bc} & L_c & -\mu M_{bc} \\ \mu L_a & \mu M_{ab} & \mu M_{bc} & -\mu^2 L_a \end{bmatrix}.$$

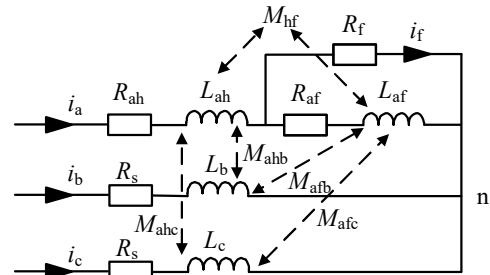


Fig. 1. Stator winding after ITSCF.

It can be observed that the asymmetric voltage components appear in the 3-phase voltages after the ITSCF. By comparing the 3-phase voltage equations before and after the fault, the 3-phase voltage residuals can be expressed as (4). When it is converted to the dq -axis frame, the second harmonic of dq -axis current and voltage can be detected, which is often used to identify ITSCF under LF [19], [20].

$$\begin{cases} u_{an} = -\mu i_f R_s - \mu \frac{d(L_a i_f)}{dt} \\ u_{bn} = -\mu \frac{d(M_{ab} i_f)}{dt} \\ u_{cn} = -\mu \frac{d(M_{ac} i_f)}{dt} \end{cases} \quad (4)$$

where Δu_{an} , Δu_{bn} , Δu_{cn} are phase voltage residuals.

The voltage residuals are primarily dependent on the machine parameters, the ratio of the faulty turns, and the operating state of the machine. Due to the fact that the fault current is positively correlated with speed and load of the machine, it can be seen that the voltage residual is relatively small when the machine operates under low speed and light load conditions, which is also the difficulty of ITSCF detection.

To achieve significant diagnostic results, the differential item of (4) is used to amplify the voltage residuals. If a 3-phase symmetrical HF voltage is injected into the machine drive system, as shown in Fig. 2, HF component will appear in the fault current and the voltage residuals will be amplified due to the increased di/dt . To ensure the balance of the system in healthy state, a 3-phase symmetrical HF voltage is injected into the system, as shown in (5).

$$\begin{cases} u_{ah} = u_h \cos \theta_h \\ u_{bh} = u_h \cos \left(\theta_h - \frac{2}{3} \pi \right) \\ u_{ch} = u_h \cos \left(\theta_h + \frac{2}{3} \pi \right) \end{cases} \quad (5)$$

where u_{ah} , u_{bh} , u_{ch} are the 3-phase HF voltage, respectively; u_h and θ_h are HF voltage amplitude and phase angle,

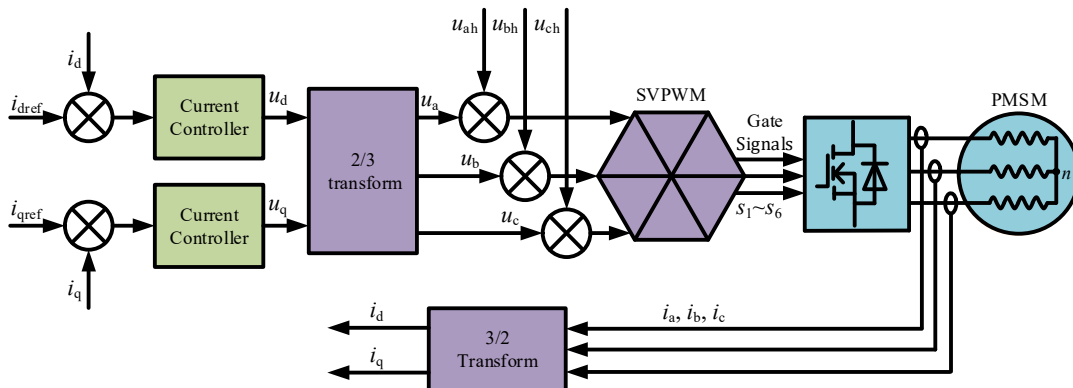


Fig. 2. The control diagram of PM machine with HF voltage injection.

respectively.

HF phase current and phase voltage are generated due to the injection of HF voltage [26], thus, there will be HF component in the short-circuit current at the injection frequency when ITSCF occurs. The fault current after the fault can be written as (6). It can be seen that there are fundamental frequency component and HF component at the injection frequency in fault current, which leads to voltage residuals at both LF and HF. Focusing on HF component only, the resistance and variations in inductance are relatively small compared to the variations in fault current, the voltage residual under HF can be simplified as (7).

$$i_f = I_{f1} \sin(\theta_h + \alpha_1) + I_{fh} \sin(\theta_h + \alpha_h) \quad (6)$$

where I_{f1} and I_f are the fundamental frequency and the HF amplitude at the injection frequency, respectively; α_1 and α_h are the phase angle of the short-circuit current.

$$\begin{cases} u_{an} = -\mu L_a I_{fh} \omega_h \cos(\theta_h + \alpha_h) \\ u_{bn} = -\mu M_{ab} I_{fh} \omega_h \cos(\theta_h + \alpha_h) \\ u_{cn} = -\mu M_{ac} I_{fh} \omega_h \cos(\theta_h + \alpha_h) \end{cases} \quad (7)$$

It can be seen that the HF component at the injection frequency is present in the 3-phase voltage residuals, and the HF voltage residual of the fault phase is the most prominent. The HF voltage residuals of the healthy phases are relatively minor, indicating that the differences of 3-phase HF voltage residuals can be utilized to detect ITSCF. Moreover, the HF voltage residuals of healthy phases may differ due to the fact that the relationship between machine parameters and fault turns, as mentioned in (2), is not strictly applicable for machines with intricate windings [28]. Therefore, the differences in 3-phase HF voltage residuals may have more significance than what has been theoretically derived.

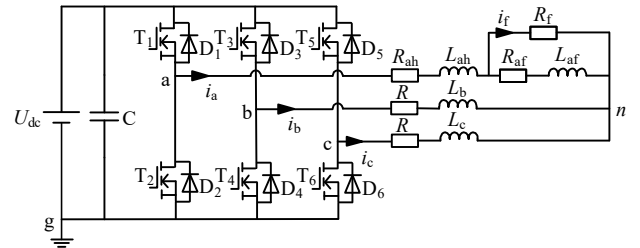


Fig. 3. 3-phase inverter circuit.

III. FAULT DIAGNOSIS

A. HF Voltage Residual Estimation

Although the HF voltage injected into the machine control system is 3-phase symmetrical, the voltage applied to the stator windings may be asymmetrical due to the loss of symmetry in the 3-phase windings under ITSCF conditions. Therefore, the reference voltage still needs to be required in real-time instead of simply using the HF voltage injected to the system. To save hardware costs and avoid adding voltage sensors, this paper estimates the reference voltage using the neutral-to-ground voltage of the bridge arm. According to the 3-phase inverter circuit, as shown in Fig. 3, the neutral-to-ground voltage of the bridge arm can be written as:

$$\begin{cases} u_{ag} = s_1 U_{dc} \\ u_{bg} = s_3 U_{dc} \\ u_{cg} = s_5 U_{dc} \end{cases} \quad (8)$$

where u_{ag} , u_{bg} , u_{cg} , are the midpoint-to-ground voltages of the bridge arm, respectively; s_1 , s_3 , s_5 are the driving signal of the upper arm power devices, respectively; u_{dc} is the dc-link voltage.

However, in actual machine drive systems, the switching frequency of the driving signal is the same as the sampling frequency, making it difficult to directly obtain it from the control system. To solve this problem, this article uses the duty cycle to obtain midpoint-to-ground voltages of the bridge arm, which can be written as:

$$\begin{cases} u_{ag} = D_a u_{dc} \\ u_{bg} = D_b u_{dc} \\ u_{cg} = D_c u_{dc} \end{cases} \quad (9)$$

where D_a , D_b , D_c are the duty cycle of the upper arm power devices, respectively.

In addition, the following relationship exists in the 3-phase inverter circuit:

$$\begin{cases} u_{ag} = u_{an} + u_{ng} \\ u_{bg} = u_{bn} + u_{ng} \\ u_{cg} = u_{cn} + u_{ng} \end{cases} \quad (10)$$

where u_{ng} is the zero-sequence voltage.

Combined with (9), (10), the reference voltage of the 3-phase windings can be calculated for both healthy and faulty conditions. When the machine works in healthy conditions, the sum of 3-phase voltages is basically zero, and the 3-phase reference voltages u_{an}^H , u_{bn}^H , u_{cn}^H can be expressed as (11). However, when the machine ITSCF occurs, the 3-phase windings are no longer symmetrical, and the sum of 3-phase voltages can be represented by (12). Based on (11) and (12), the 3-phase reference voltages after the ITSCF u_{an}^{TF} , u_{bn}^{TF} , u_{cn}^{TF} can be deduced as (13).

$$\begin{bmatrix} u_{an}^H \\ u_{bn}^H \\ u_{cn}^H \end{bmatrix} = \frac{1}{3} \begin{bmatrix} 2 & -1 & -1 \\ -1 & 2 & -1 \\ -1 & -1 & 2 \end{bmatrix} \begin{bmatrix} u_{ag} \\ u_{bg} \\ u_{cg} \end{bmatrix} \quad (11)$$

$$\Delta u_{an} + \Delta u_{bn} + \Delta u_{cn} = -\mu i_f R_s - \mu \frac{d(L_{ls} i_f)}{dt} \quad (12)$$

where L_{ls} is the leakage inductance.

$$\begin{bmatrix} u_{an}^{TF} \\ u_{bn}^{TF} \\ u_{cn}^{TF} \end{bmatrix} = \begin{bmatrix} u_{an}^H \\ u_{bn}^H \\ u_{cn}^H \end{bmatrix} - \frac{1}{3} \left(\mu i_f R_s + \mu \frac{d(L_{ls} i_f)}{dt} \right) \begin{bmatrix} 1 \\ 1 \\ 1 \end{bmatrix} \quad (13)$$

Compared with the 3-phase voltages in healthy mode, there is an additional zero-sequence voltage component in the 3-phase reference voltages after the ITSCF. Note that the voltage offset caused by the zero-sequence voltage is the same in 3-phase windings. Therefore, the voltage offset can be ignored and the 3-phase voltages before and after the ITSCF can be calculated using (10). Although this will cause a certain error after ITSCF, the same error exists in the three phases and will not cause extra imbalance between the 3-phase windings.

When estimating the phase voltage of PMSM, commonly used methods include table lookup and direct calculation. The table lookup method requires obtaining the voltage of machine through finite element simulation or experiment testing and performing interpolation estimation. However, this approach necessitates a substantial amount of simulation or experimental data, which is not suitable for the diagnosis of unknown faults. Therefore, this paper employs the direct calculation method to estimate the phase voltage. Although the calculation of differential items can be susceptible to noise, the filtering measures required for extracting the HF component can offset this impact. The dq -axis estimated voltage u_{d_e} , u_{q_e} can be expressed as follows:

$$\begin{bmatrix} u_{d_e} \\ u_{q_e} \end{bmatrix} = \begin{bmatrix} R_s & 0 \\ 0 & R_s \end{bmatrix} \begin{bmatrix} i_d \\ i_q \end{bmatrix} + \begin{bmatrix} L_d & 0 \\ 0 & L_q \end{bmatrix} \begin{bmatrix} \frac{di_d}{dt} \\ \frac{di_q}{dt} \end{bmatrix} + \omega_e \begin{bmatrix} 0 & -L_q \\ L_d & 0 \end{bmatrix} \begin{bmatrix} i_d \\ i_q \end{bmatrix} + \omega_e \begin{bmatrix} 0 \\ \varphi_m \end{bmatrix} \quad (14)$$

where u_d and u_q are the dq -axis voltages, respectively.

According to reverse Park transformation, the 3-phase estimated voltages u_{an_e} , u_{bn_e} , u_{cn_e} can be written as:

$$\begin{bmatrix} u_{an_e} & u_{bn_e} & u_{cn_e} \end{bmatrix}^T = \mathbf{T}(\theta) \begin{bmatrix} u_{d_e} & u_{q_e} \end{bmatrix}^T \quad (15)$$

$$\mathbf{T}(\theta) = \begin{bmatrix} \cos \theta & -\sin \theta \\ \cos \left(\theta - \frac{2}{3} \pi \right) & -\sin \left(\theta - \frac{2}{3} \pi \right) \\ \cos \left(\theta + \frac{2}{3} \pi \right) & -\sin \left(\theta + \frac{2}{3} \pi \right) \end{bmatrix} \quad (16)$$

Traditional band pass filters face difficulty in extracting a single frequency, and hence the frequency tracking algorithm proposed in [15] is utilized to extract the HF amplitude of both the reference voltage and estimated voltage at the injection frequency, as shown in Fig. 4. The amplitude of the reference voltage denote as $U_{an_r}^{HF}$, $U_{bn_r}^{HF}$, and the amplitude of the estimated voltage denote as $U_{an_e}^{HF}$, $U_{bn_e}^{HF}$, $U_{cn_e}^{HF}$. Based on the

3-phase HF reference voltages and 3-phase HF estimated voltages, the 3-phase HF voltage residuals ΔU_{an}^{HF} , ΔU_{bn}^{HF} , ΔU_{cn}^{HF} can be expressed as:

$$\begin{cases} U_{an}^{HF} = U_{an_r}^{HF} - U_{an_e}^{HF} \\ U_{bn}^{HF} = U_{bn_r}^{HF} - U_{bn_e}^{HF} \\ U_{cn}^{HF} = U_{cn_r}^{HF} - U_{cn_e}^{HF} \end{cases} \quad (17)$$

The definition of the fault indicator should ensure that misdiagnosis does not occur in the healthy state and that a prompt warning can be given in the fault state. Since the 3-phase voltage residuals caused by errors in the healthy condition are basically the same, which will be analyzed in the next section. To represent the dispersion degree of 3-phase HF voltage residuals after the fault, the fault indicator is defined as the standard deviation of the HF voltage, which can be written as:

$$FI = \sqrt{\frac{(\Delta U_{an}^{HF} - k)^2 + (\Delta U_{bn}^{HF} - k)^2 + (\Delta U_{cn}^{HF} - k)^2}{3}} \quad (18)$$

in which

$$k = \frac{1}{3}(\Delta U_{an}^{HF} + \Delta U_{bn}^{HF} + \Delta U_{cn}^{HF}) \quad (19)$$

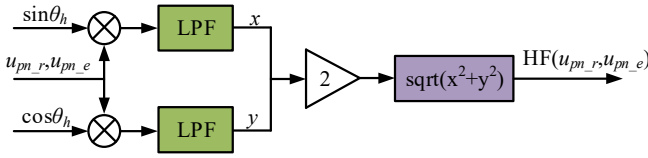


Fig. 4. HF component extraction strategy.

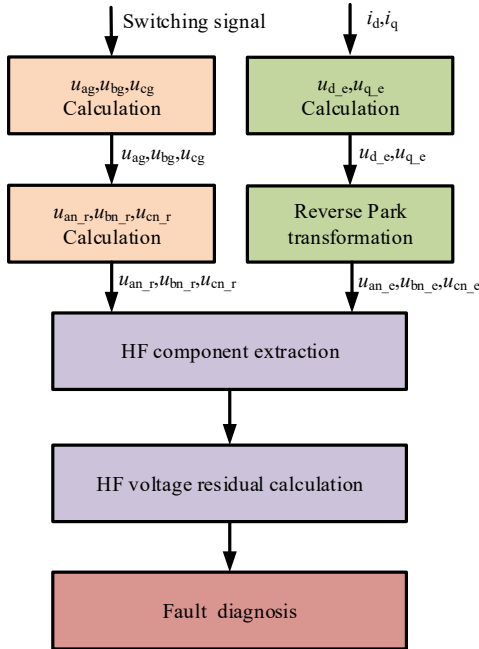


Fig. 5. Inter-turn fault detection strategy.

When the machine operates normally, the HF components of the reference phase voltages are essentially the same as the HF components of the estimated phase voltages. Hence, the HF voltage residuals and the fault indicator are basically zero. After the fault, the HF components of the reference phase

voltages will deviate from the HF components of the estimated phase voltages due to the presence of voltage residuals. As a result, the HF voltage residuals and the fault indicator increase rapidly, clearly indicating the occurrence of ITSCF.

Based on the analysis above, the flowchart of the ITSCF diagnosis based on HF voltage residual is presented in Fig. 5. Initially, the reference voltage signals are computed using the duty cycle of the power device, and the actual voltage signals are estimated using the voltage equation. Then, the HF components of the both reference and the actual voltage signals are extracted. Finally, the HF voltage residuals are calculated to achieve ITSCF diagnosis.

B. Parameter Variation Analysis

It can be observed that HF voltage residuals are significantly related to the machine parameters that may vary under different operating conditions. For instance, the resistance of stator winding may rise as the temperature increases, while the inductance may decrease as a result of magnetic circuit saturation. Therefore, it is crucial to examine how changes in machine parameters impact the diagnostic method. Under HF conditions, the ratio of resistance voltage and back EMF is relatively insignificant and can be neglected. As a result, only the influence of dq -axis inductances is taken into consideration. When the dq -axis inductances vary to $L_d + \Delta L_d$, $L_q + \Delta L_q$, the dq -axis voltage equations can be expressed as:

$$\begin{bmatrix} u_d \\ u_q \end{bmatrix} = \begin{bmatrix} L_d + \Delta L_d & 0 \\ 0 & L_q + \Delta L_q \end{bmatrix} \begin{bmatrix} \frac{di_d}{dt} & \frac{di_q}{dt} \end{bmatrix}^T \quad (20)$$

where ΔL_d and ΔL_q are the variations of dq -axis inductances, respectively.

The residual of dq -axis voltages caused by parameter changes can be expressed as:

$$\begin{bmatrix} \Delta u_d \\ \Delta u_q \end{bmatrix} = \begin{bmatrix} \Delta L_d & 0 \\ 0 & \Delta L_q \end{bmatrix} \begin{bmatrix} \frac{di_d}{dt} & \frac{di_q}{dt} \end{bmatrix}^T \quad (21)$$

To analyze the influence of dq -axis inductances on 3-phase voltages, (20) is transformed into 3-phase frame, which can be written as:

$$\begin{bmatrix} \Delta u_{an} \\ \Delta u_{bn} \\ \Delta u_{cn} \end{bmatrix}^T = \mathbf{T}(\theta) \begin{bmatrix} \Delta u_d \\ \Delta u_q \end{bmatrix}^T \quad (22)$$

While changes in parameter can result in residual changes in 3-phase voltages, the 3-phase voltage residuals remain symmetrical. Therefore, the amplitudes of 3-phase HF voltage residuals are still equal. As per (18), it will not trigger the fault indicator signal.

C. Error Analysis

As the duty cycle is the proportion of the power device on-time to the switching cycle, (9) yields the average value of the midpoint-to-ground voltage in a switching cycle. Unlike the driving signal, the duty cycle and phase current only maintain the corresponding relationship within one switching period, which implies that the reference voltage and the actual voltage do not always correspond.

Furthermore, inaccuracies in reference voltage and estimated voltage can arise due to non-ideal factors such as the switching

characteristic of power devices and the sampling delay of current sensors. However, the errors caused by these effects on 3-phase system are essentially identical under normal operating conditions. Thus, there might be 3-phase HF voltage residuals with the same amplitude under normal conditions. Based on the definition of the fault indicator, the HF voltage residual caused by errors will not result in misdiagnosis.

D. Transient Analysis

According to the above analysis, the HF current will be generated due to the injection of HF voltage. However, owing to the low control bandwidth of the current controller, the HF current is not involved in the control process of the system, which means that the HF reference voltage is generated solely by the injection signal and is not affected by the control system. Furthermore, the fault diagnosis method proposed in this paper uses phase current to calculate estimated voltages, but only the 3-phase HF estimated voltages are required, which are generated by 3-phase HF current and independent of the fundamental frequency current. Therefore, despite abruptly changes in the fundamental frequency signal during the transient process of the machine, the HF voltage residuals remain basically constant.

E. Detection Region Analysis

The proposed method is not significantly restricted by the operating frequency of the machine since the injected signal frequency is much higher. However, it should be considered that when the machine operates at high speeds in the flux-weakening region, the amplitude of the injected HF voltage may be affected by various factors such as the DC-link voltage and machine EMF. This means that the proposed method may be impacted when the machine operates at limited speeds. Nevertheless, this impact is typically negligible since the amplitude of the injected HF voltage is usually kept low to minimize the HF noise caused by the injection. Additionally, it is worth noting that the HF injection method is generally applied at low speeds of the machine, as the fundamental frequency fault characteristics are already prominent at high speeds [18], [19]. Therefore, the issues encountered by the HF injection-based fault diagnosis method in the flux-weakening region can be largely ignored, and the proposed method can adequately meet the health monitoring needs of the machine during operation.

IV. EXPERIMENTAL RESULTS

This paper employs a triple 3-phase PMSM to validate the proposed method, as shown in Fig. 6. The phase winding of the machine consists of two coils that are connected in series with 30° phase shift between them. The specifications of the machine are listed in Table I. In comparison with the traditional PMSM, the triple 3-phase PMSM has three independent 3-phase winding modules and possesses stronger fault-tolerant capability. The experiment setup of the triple 3-phase PMSM is illustrated in Fig. 7, which mainly comprises the triple 3-phase PMSM, dynamometer and control circuit. Both the switching frequency and sampling frequency are set to 10 kHz. The PMSM is linked to the dynamometer via a torque transducer and operates in current loop

mode. Additionally, the ITSCF is accomplished by introducing two taps on one turn of the phase B winding, as depicted in Fig. 8. During the experiment, the relay switch is controlled to achieve the transition between the healthy and inter-turn fault states.

TABLE I
MACHINE SPECIFICATIONS

Specification	Symbol	Value
Rated speed	n_N	2000 rpm
Rated power	P	5 kW
Rated current	I_N	67 A
PM flux linkage	ψ_m	0.015 Wb
d -axis inductance	L_d	0.29 mH
q -axis inductance	L_q	0.92 mH
Stator resistance	R_s	0.022 Ω
Pair of poles	p_r	3
Turn number of each coil	N	8
Number of faulted turns	N_f	1

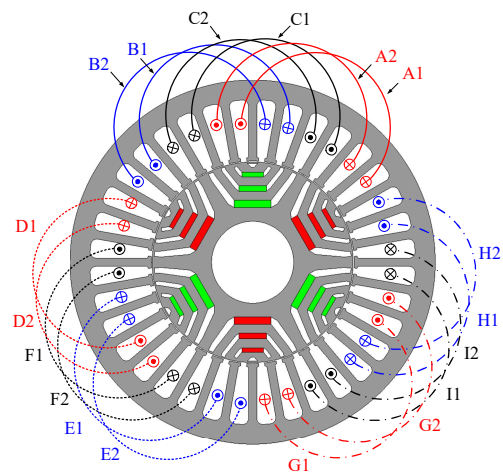


Fig. 6. Triple 3-phase PMSM.

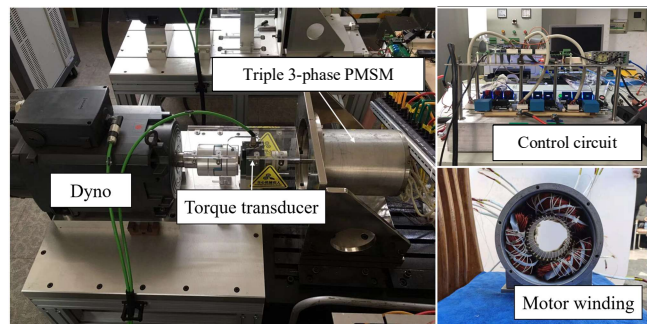


Fig. 7. Experimental setup of triple 3-phase PMSM.

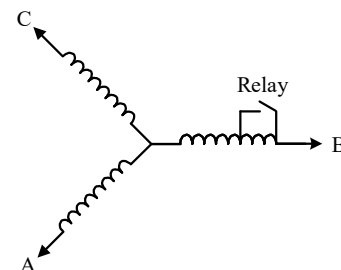


Fig. 8. Schematic diagram of ITSCF.

A. Fault Diagnosis

A high fault current is produced in the short-circuit winding when ITSCF occurs in the machine. Fig. 9 presents the fault current waveform when the machine operates at 500 rpm with 10 A load. It is apparent that the fault current has attained the rated value. It will be expected to be several times of the rated value if operation at higher speed with larger current. To ensure the safety of the machine and its drive system, this paper only conducted tests at or below under half of the rated state.

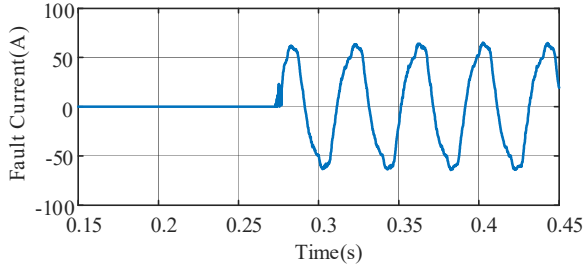


Fig. 9. Fault current waveform of machine at 500 rpm with 10 A load.

To achieve an optimal diagnostic effect, a 1200 Hz HF voltage is injected into the control system. Taking the fault phase as an example, Fig. 10 and Fig. 11 demonstrate the FFT analysis results of the reference voltage and estimated voltage before and after the fault, respectively. In healthy conditions, there is a certain difference between the HF components of reference voltages and the estimated voltages, which may be caused by sampling delays and parameter mismatches. However, the residuals of the three phases are essentially the same. After the fault occurs, there is a significant difference between the reference voltage and estimated voltage of the three phases, with the fault phase exhibiting the largest voltage residual. It should be noted that the reference voltage also changed after the turn fault, which is caused by the shift of the neutral point voltage.

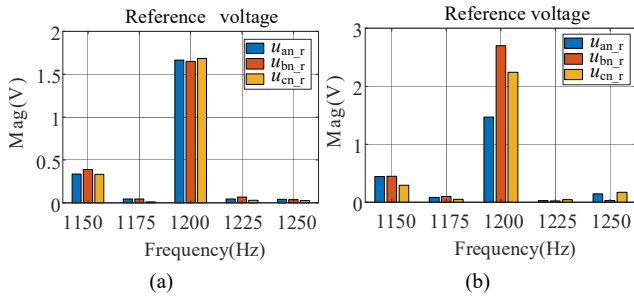


Fig. 10. FFT analysis results of reference voltage before and after the fault. (a) Before the fault. (b) After the fault.

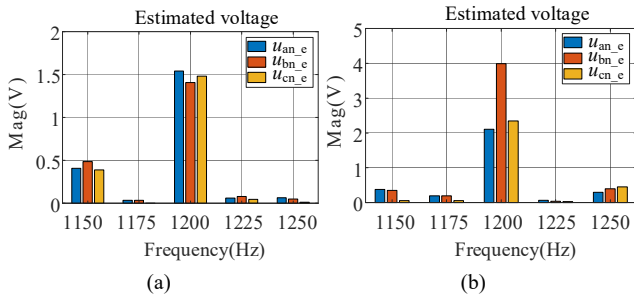


Fig. 11. FFT analysis results of estimated voltage before and after the fault. (a) Before the fault. (b) After the fault.

Fig. 12 presents the experimental results of the ITSCF that occurred while the machine operates at the operating point of 500 rpm with 10 A load. It is apparent that the 3-phase current exhibits only minor changes before and after the fault, making it challenging to detect the fault directly. However, there is a significant difference in the residual of the 3-phase HF voltage before and after the fault, which can be utilized to detect the ITSCF. Additionally, the voltage residual amplitude of the fault phase is the largest and can be utilized to locate the position of the fault.

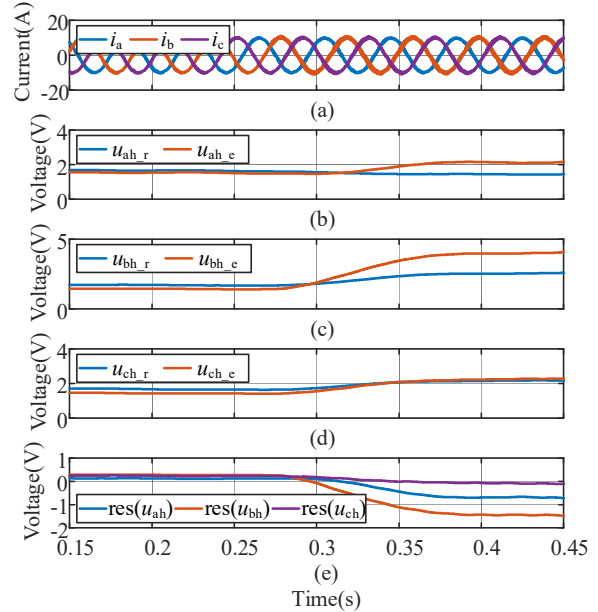


Fig. 12. Fault diagnosis at 500 rpm with 10 A load. (a) 3-phase currents. (b) Phase A HF voltage. (c) Phase B HF voltage. (d) Phase C HF voltage. (e) Fault indicator.

Fig. 13 displays the waveform of dq -axis current and reference voltage before and after the fault. It is evident that the dq -axis current and reference voltage can be considered as a direct current before the fault, and there is a small second harmonic after the fault. Fig. 14 illustrates the waveform of dq -axis voltage residual. Similar to dq -axis current and reference voltage, the second harmonic of voltage residual also experiences a slight increase after the fault. However, the second harmonic content is relatively low and varies with the running state of the machine, which makes it unsuitable as a stable fault indicator.

Similarly, the test is also conducted under the condition that the machine operates at 1000 rpm with 30 A load, as shown in

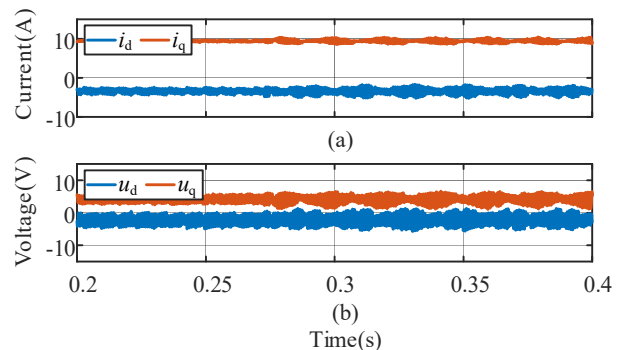


Fig. 13. The waveform of dq -axis current and reference voltage. (a) dq -axis current. (b) dq -axis reference voltage.

Fig. 15. It is observed that after ITSCF, the 3-phase HF voltage residuals still change rapidly, causing the fault indicator to quickly rise, indicating the presence of ITSCF. The above results demonstrated that the method proposed in this paper can be applied under different operating conditions of the machine.

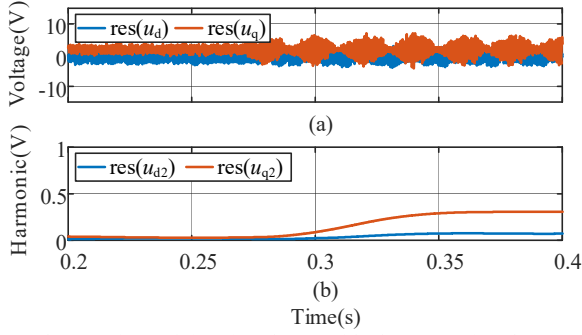


Fig. 14. The waveform of dq -axis voltage residual. (a) dq -axis voltage residual. (b) The second harmonic of dq -axis voltage residual.

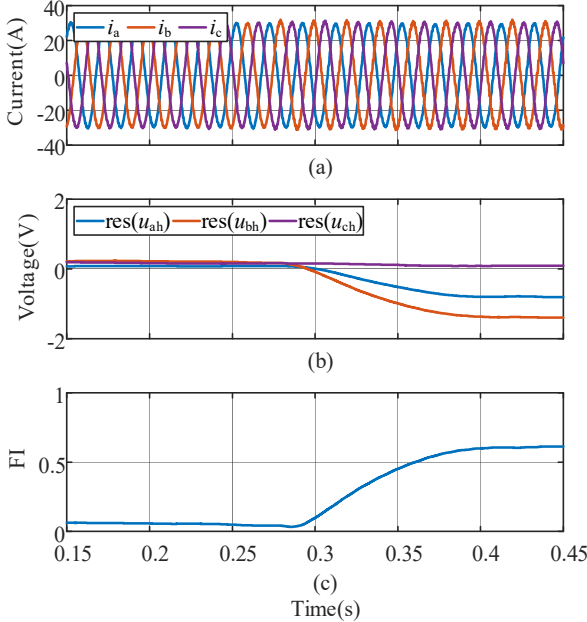


Fig. 15. Fault diagnosis at 1000 rpm with 30 A load. (a) 3-phase currents (b) HF voltage residual. (c) Fault indicator.

B. Transient Process

The variation of the fault indicator in the transient process of the machine is a critical index to evaluate the fault diagnosis method. Fig. 16 presents the experimental results of machine loading at 1000 rpm. The results demonstrate that the 3-phase currents undergo transient changes from 10 A to 30 A, but the 3-phase HF voltage residuals of the machine remain almost constant during loading. Hence, the fault diagnosis method proposed in this paper is minimally affected by the transient process of the machine, which is also a significant advantage over the LF signal-based diagnosis method.

C. Parameter Mismatch

As a model-based fault diagnosis method, the influence of the parameters is also verified when the machine works at 1000 rpm with 10 A load, as shown in Fig. 17. In the experiment, the d -axis inductance utilized in the calculations is reduced by 20%.

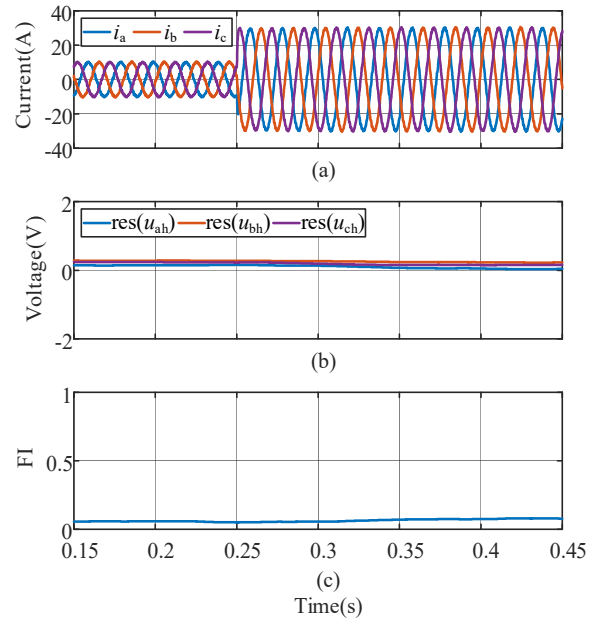


Fig. 16. The loading waveform of the machine at 1000 rpm. (a) 3-phase currents. (b) HF voltage residual. (c) Fault indicator.

Compared with Fig. 11, it can be observed that the amplitude of the 3-phase HF voltage residuals changes slightly in the healthy condition. Although the amplitudes of the 3-phase HF voltage residuals are affected by the machine parameters, it can be seen that the 3-phase HF voltage residuals are still essentially equal, which will not lead to misdiagnosis. After the fault, the amplitude of the 3-phase voltage residuals is no longer the same, and the diagnosis of ITSCF can still be achieved.

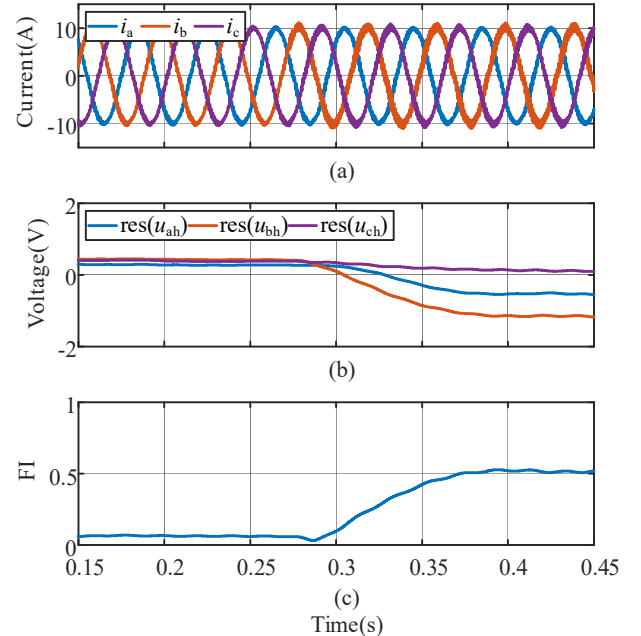


Fig. 17. Experimental waveform of d -axis inductance reduction. (a) 3-phase currents. (b) HF voltage residual. (c) Fault indicator.

V. CONCLUSION

In this paper, an ITSCF diagnosis method based on HF voltage residual is proposed. The voltage residuals are analyzed for both HF and LF conditions. It is demonstrated that the

voltage residual can be enhanced under HF voltage injection. Extensive experiments verify the effectiveness of the proposed method, and the following conclusions are drawn.

1) The ITSCF diagnosis method based on HF voltage is reliable in detecting faults across all operation ranges, including low speed and light load conditions, which are historically the most challenging for inter-turn fault detection.

2) The HF voltage residual exhibits more pronounced fault signatures in contrast to conventional diagnosis methods.

3) The fault diagnosis method of HF voltage residual is highly robust, as it is not affected by the transient processes or parameter variations.

Furthermore, this method shows a certain ability to distinguish high resistance fault, which is unattainable with traditional diagnosis method under LF. This will be reflected in future research.

REFERENCES

- [1] M. Hermance, Y. Gao, and J. M. Miller, "Hybrid Electric Vehicles: Architecture and Motor Drives," *Proc. IEEE*, vol. 95, no. 4, pp. 719-728, Apr. 2007.
- [2] B. Wang, J. Hu, and W. Hua *et al*, "Fault Operation Analysis of a Triple-redundant Three-phase PMA-SynRM for EV Application," *IEEE Trans. Transport. Electric.*, vol. 7, no. 1, pp. 183-192, March 2021.
- [3] H. Chen, N. A. O. Demerdash, and A. M. EL-Refaie, *et al*, "Investigation of a 3D-Magnetic Flux PMSM with High Torque Density for Electric Vehicles," *IEEE Trans. Energy Convers.*, vol. 37, no. 2, pp. 1442-1454, June 2022.
- [4] P. O'Donnell, "Report of large motor reliability survey of industrial and commercial installations, part 1," *IEEE Trans. Ind. Appl.*, vol. IA-21, no. 4, pp. 853-864, Jul. 1985.
- [5] A. Siddique, G. S. Yadava and B. Singh, "A Review of Stator Fault Monitoring Techniques of Induction Motors," *IEEE Trans. Energy Convers.*, vol. 20, no. 1, pp. 106-114, March 2005.
- [6] S. Grubic, J. M. Aller, and B. Lu *et al*, "A Survey on Testing and Monitoring Methods for Stator Insulation Systems of Low-voltage Induction Machines Focusing on Turn Insulation Problems," *IEEE Trans. Ind. Electron.*, vol. 55, no. 12, pp. 4127-4136, Dec. 2008.
- [7] B. Wang, J. Wang, and A. Griffo *et al*, "A Turn Fault Mitigation Strategy Based on Current Injection Technique for a Triple Three-phase PMA SynRM," *IEEE Trans. Ind. Electron.*, vol. 67, no. 4, pp. 2511-2522, April 2020.
- [8] B. Wang, X. Feng, and J. Bao *et al*, "A Low Coupling Fault Tolerant PMA-SynRM With Mixed-Pitch Segregated Windings," *IEEE Trans. Transport. Electric.*, vol. 8, no. 4, pp. 4549-4559, Dec. 2022.
- [9] L. Geng, F. Chai, and Y. Pei, "Mitigation of Interturn Short Circuit Fault Based on Axial Split Phase Permanent Magnet Synchronous Machine," *IEEE Trans. Energy Convers.*, vol. 37, no. 4, pp. 2578-2587, Dec. 2022.
- [10] J. Dusek, P. Arumugam, and C. Brunson *et al*, "Impact of Slot/Pole Combination on Inter-Turn Short-circuit Current in Fault-tolerant Permanent Magnet Machines," *IEEE Trans. Mag.*, vol. 52, no. 4, pp. 1-9, April 2016.
- [11] J. Hang, W. Sun, and Q. Hu *et al*, "Integration of Interturn Fault Diagnosis and Fault-tolerant Control for PMSM Drive System," *IEEE Trans. Transport. Electric.*, vol. 8, no. 2, pp. 2825-2835, June 2022.
- [12] J. Hang, S. Ding, and X. Ren *et al*, "Integration of Interturn Fault Diagnosis and Torque Ripple Minimization Control for Direct-Torque-Controlled SPMSM Drive System," *IEEE Trans. Power Electron.*, vol. 36, no. 10, pp. 11124-11134, Oct. 2021.
- [13] R. Z. Haddad and E. G. Strangas, "On the Accuracy of Fault Detection and Separation in Permanent Magnet Synchronous Machines Using MCSA/MVSA and LDA," *IEEE Trans. Energy Convers.*, vol. 31, no. 3, pp. 924-934, Sept. 2016.
- [14] J. A. Rosero, L. Romeral, and J. A. Ortega *et al*, "Short-circuit Detection by Means of Empirical Mode Decomposition and Wigner-ville

Distribution for PMSM Running Under Dynamic Condition," *IEEE Trans. Ind. Electron.*, vol. 56, no. 11, pp. 4534-4547, Nov. 2009.

- [15] J. Hang, J. Zhang, and M. Cheng *et al*, "Online Interturn Fault Diagnosis of Permanent Magnet Synchronous Machine Using Zero-sequence Components," *IEEE Trans. Power Electron.*, vol. 30, no. 12, pp. 6731-6741, Dec. 2015.
- [16] A. Alloui, K. Laadjal, and M. Sahraoui *et al*, "Online Interturn Short-circuit Fault Diagnosis in Induction Motors Operating Under Unbalanced Supply Voltage and Load Variations, Using the STLSP Technique," *IEEE Trans. Ind. Electron.*, vol. 70, no. 3, pp. 3080-3089, March 2023.
- [17] H. Jeong, S. Moon, and S. W. Kim, "An Early Stage Interturn Fault Diagnosis of PMSMs by Using Negative-Sequence Components," *IEEE Trans. Ind. Electron.*, vol. 64, no. 7, pp. 5701-5708, July 2017.
- [18] R. Hu, J. Wang, and A. R. Mills *et al*, "Current-residual-based Stator Interturn Fault Detection in Permanent Magnet Machines," *IEEE Trans. Ind. Electron.*, vol. 68, no. 1, pp. 59-69, Jan. 2021.
- [19] J. Hang, Q. Hu and W. Sun *et al*, "A Voltage-Distortion-Based Method for Robust Detection and Location of Interturn Fault in Permanent Magnet Synchronous Machine," *IEEE Trans. Power Electron.*, vol. 37, no. 9, pp. 11174-11186, Sept. 2022.
- [20] M. Zafarani, E. Bostanci, and Y. Qi *et al*, "Interturn Short-circuit Faults in Permanent Magnet Synchronous Machines: An Extended Review and Comprehensive Analysis," *IEEE J. Emerg. Sel. Topics Power Electron.*, vol. 6, no. 4, pp. 2173-2191, Dec. 2018.
- [21] Z. Xu, J. Zhang, and Y. Zhang *et al*, "Winding Condition Monitoring for Inverter-fed PMSM Using High-Frequency Current Injection," *IEEE Trans. Ind. Appl.*, vol. 57, no. 6, pp. 5818-5828, Nov.-Dec. 2021.
- [22] J. Zhang, Z. Xu, and J. Wang *et al*, "Detection and Discrimination of Incipient Stator Faults for Inverter-fed Permanent Magnet Synchronous Machines," *IEEE Trans. Ind. Electron.*, vol. 68, no. 8, pp. 7505-7515, Aug. 2021.
- [23] B. Wang, L. Luo, and W. Fu *et al*, "Study on the PWM Ripple Current Based Turn Fault Detection for Interior PM Machine," *IEEE Trans. Transport. Electric.*, vol. 7, no. 3, pp. 1537-1547, Sept. 2021.
- [24] B. Sen, and J. Wang, "Stator Interturn Fault Detection in Permanent-Magnet Machines Using PWM Ripple Current Measurement," *IEEE Trans. Ind. Electron.*, vol. 63, no. 5, pp. 3148-3157, May 2016.
- [25] G. Zanusso, S. L. S. Kumar, and L. Peretti, "Interturn Fault Detection in Induction Machines Based on High-Frequency Injection," *IEEE Trans. Ind. Electron.*, to be published, doi: 10.1109/TIE.2022.3217590.
- [26] R. Hu, J. Wang, and A. R. Mills *et al*, "High-frequency Voltage Injection Based Stator Interturn Fault Detection in Permanent Magnet Machines," *IEEE Trans. Power Electron.*, vol. 36, no. 1, pp. 785-794, Jan. 2021.
- [27] Y. Qi, E. Bostanci, and V. Gurusamy *et al*, "A Comprehensive Analysis of Short-Circuit Current Behavior in PMSM Interturn Short-circuit Faults," *IEEE Trans. Power Electron.*, vol. 33, no. 12, pp. 10784-10793, Dec. 2018.
- [28] B. Vaseghi, B. Nahid-mobarakh, and N. Takorabet *et al*, "Inductance Identification and Study of PM Motor with Winding Turn Short Circuit Fault," *IEEE Trans. Magn.*, vol. 47, no. 5, pp. 978-981, May 2011.



Xiaobao Feng received the B.S. degree in electrical engineering from the Tianjin University of Science and Technology, Tianjin, China, in 2018 and the M.S. degrees in electrical engineering from the Nanjing University of Aeronautics and Astronautics, Nanjing, China, in 2021. Now he is currently working toward the Ph.D. degree in electrical engineering at Southeast University, Nanjing, China.

His research interests include power converters and electrical machine driving systems.



Bo Wang (SM'23) received the B.Eng. and M.Sc. degrees in Electrical Engineering from Nanjing University of Aeronautics and Astronautics, Nanjing, China, in 2009 and 2012, respectively and the Ph.D. degree in Electronic and Electrical Engineering from the University of Sheffield, Sheffield, U.K., in 2018.

From 2012 to 2014, he served as a senior engineer in the Delta Electronics Co. Ltd. From 2017 to 2018, he was a research associate at the Department of Electronic and Electrical Engineering, University of Sheffield. Since 2018, he has joined the School of Electrical Engineering, Southeast University as an Associate Research Fellow. From 2020 to 2022, he joined Hong Kong Poly U under the Hong Kong Scholar program. His research interests include the permanent magnet machine drives, electric traction and fault tolerant systems.



Zheng Wang (S'05–M'09–SM'14) received the B.Eng. and M. Eng. degrees from Southeast University, Nanjing, China, in 2000 and 2003, respectively, and the Ph.D. degree from The University of Hong Kong, Hong Kong, in 2008, all in electrical engineering.

From 2008 to 2009, he was a Postdoctoral Fellow in Ryerson University, Toronto, ON, Canada. He is currently a full Professor in the School of Electrical Engineering, Southeast University, China. His research interests include electric drives, power electronics, and distributed generation. He has authored or coauthored over 100 internationally refereed papers and four books in these areas.

Prof. Wang received several academic awards including IEEE PES Chapter Outstanding Engineer Award, Jiangsu Outstanding Young Scholar Award and four Best/Outstanding Paper Awards. He is an Associate Editor of IEEE Trans. on Industrial Electronics and Journal of Power Electronics.



Chaohui Liu (Member, IEEE) received the B.E. degree from the North University of China, the M.E degree from Beihang University, Beijing, China, and the Ph.D. degree from the Electrical Machines and Drives (EMD) Research Group, University of Sheffield, Sheffield, U.K., in 2006, 2011, and 2017, respectively.

From 2017 to 2020, he was with the Department of Research, Design and Development, Dyson Technology Limited, Malmesbury, U.K., where he was appointed an Advanced Engineer in 2017 and a Senior Engineer in 2018. He is currently a Principle Engineer and the Head of Powertrain with National New Energy Vehicle Technology Innovation Center (NEVC), Beijing, China. His research interests include machine drive, advanced control strategy, power converters, electric vehicle battery charger, wide band-gap device packaging, and power module applications.



Jiayun Zeng was born in Nanchang City, Jiangxi Province, Senior Engineer of Nanjing Engineering Institute of Aircraft System of Aviation Industry Corporation of China, Ltd. (AVIC NEIAS). She graduated from Nanjing University of Aeronautics and Astronautics with a master's degree in Micro-Electro-Mechanical System and

Microfabrication in 2007. Long term commitment to research on aircrafts controlling based on software engineering and process. She was once rewarded a meritorious medal of 'Aeronautical Patriotism' accordingly by AVIC.